Journal of Materials Chemistry C

ROYAL SOCIETY OF CHEMISTRY

COMMUNICATION

View Article Online
View Journal | View Issue

Cite this: J. Mater. Chem. C, 2022, 10, 17059

Received 18th September 2022,
Accepted 3rd November 2022

DOI: 10.1039/d2tc03933h

rsc.li/materials-c

Equilibrating the key parameters of thermally activated delayed fluorescence emitters towards efficient red/near-infrared OLEDs†

Jinming Fan,[ab] Yulin Xu,[a] Nengquan Li,[a] Jingsheng Miao,[a] Changjiang Zhou,[c] Tengxiao Liu,[d] Minrong Zhu[a] and Xiaojun Yin *[a]

Equilibrating the critical parameters associated with the thermally activated delayed fluorescence process proposes the prerequisite for realizing high performance electroluminescence devices. Herein, precise manipulations relying on the model near-infrared emitter are successfully demonstrated, affording improved maximum external quantum efficiencies of 18.9% (@630 nm) and 12.6% (@680 nm).

Effective utilization of the triplet excitons in organic light-emitting diodes (OLEDs) is one of the fundamental issues to adapt to the commercial requirements of high device performances and durability[1,2] since the radiative transition from triplet to ground states (S_0) in purely organic emitters is typically spin-forbidden and excess triplet excitons are the prime factor for efficiency roll-offs as well.[3–7] Recycling the dark-state triplet excitons into spin-allowed singlet excitons *via* the thermally activated reverse intersystem crossing (RISC) channel (*i.e.*, thermally activated delayed fluorescence mechanism, TADF) can fully realize the potential of organic emitters in OLEDs.[8–10] To pursue a high RISC rate constant (k_{RISC}), a small singlet–triplet energy gap (ΔE_{ST}) between the lowest singlet state (S_1) and triplet state (T_1) is one of the basic principles.[11] However, a small ΔE_{ST} requires highly separated frontier orbitals between the highest occupied molecular orbitals (HOMOs) and the lowest unoccupied molecular orbitals (LUMOs), which will inevitably bring about inefficient spin–orbit coupling (SOC) between the relevant excited states and small $S_1 \rightarrow S_0$ transition dipole moments ($|\vec{\mu}_{S_1-S_0}|$) synchronously.[11–13] Undoubtedly, an adequate balance among these key parameters (*e.g.*, k_{RISC}, ΔE_{ST}, and SOC values) that are associated with the TADF process proposes a reliable hypothesis to obtain desirable TADF emitters with high luminous efficiency, yet tremendous challenges to thoroughly equilibrate these parameters are still remaining.[14–16] In particular, the trade-off relationships are more complicated in the long wavelength emission region due to the energy gap law;[17–19] that is, the vibrational relaxation of non-radiative transition from electronically excited S_1 or T_1 to the zeroth vibration level of the S_0 state is remarkably accelerated along with the narrowing of emission gaps.[20–22]

The development of red/near-infrared (NIR) TADF materials is urgently needed, arising from the wide application prospects in OLEDs, night-vision displays, bioimaging, phototherapy, telecommunications, *etc.*[23–27] To date, multiple seminal works and new perspectives have been proposed to overcome the interference of key parameters in red/NIR-TADF emitters,[28–32] including the incorporation of the non-adiabatic coupling effect,[33,34] multi-resonance skeletons with shallow potential energy surfaces,[20] intramolecular hydrogen-bonding,[35] regulation of the locally excited and charge-transfer (CT) triplet state, *etc.*[14,36] In view of the decisive role of energy gap law for red/NIR emitters, radiative decay rate ($k_{r,s}$) of S_1 is the primary concern.[37,38] Within the typical donor–acceptor (D–A) type red/NIR TADF molecules, the triarylamine derivatives comprising free rotation phenyl groups commonly serve as the D component to endow them with low reorganization energy and high luminous efficiency.[39–43] For example, Qiao *et al.* demonstrated a high photoluminescence quantum yield (Φ_{PL}) of 97.4% (dpTPAAP) with an emission peak at 624 nm,[33] Xu and co-workers showed an excellent Φ_{PL} of 90% (*p*CNQ–TPA) with an emission peak even at 691 nm,[44] and Ma *et al.* revealed a very high oscillator strength (f) of 0.72 (DTPS-PT) for the

[a] Shenzhen Key Laboratory of New Information Display and Storage Materials, College of Materials Science and Engineering, Shenzhen University, Shenzhen, 518060, People's Republic of China. E-mail: xiaojunyin@szu.edu.cn
[b] College of Physics and Optoelectronic Engineering, Shenzhen University, Shenzhen, 518060, People's Republic of China
[c] College of Chemical Engineering, Zhejiang University of Technology, Hangzhou, 310014, P. R. China
[d] College of Chemistry and Environmental Science, Wuhan Institute of Bioengineering, Wuhan, 430415, People's Republic of China

† Electronic supplementary information (ESI) available: General information, synthetic procedures, characterization data, NMR and HRMS spectra, theoretical calculations, PL spectra, crystal and device data. CCDC 2184275. For ESI and crystallographic data in CIF or other electronic format see DOI: https://doi.org/10.1039/d2tc03933h

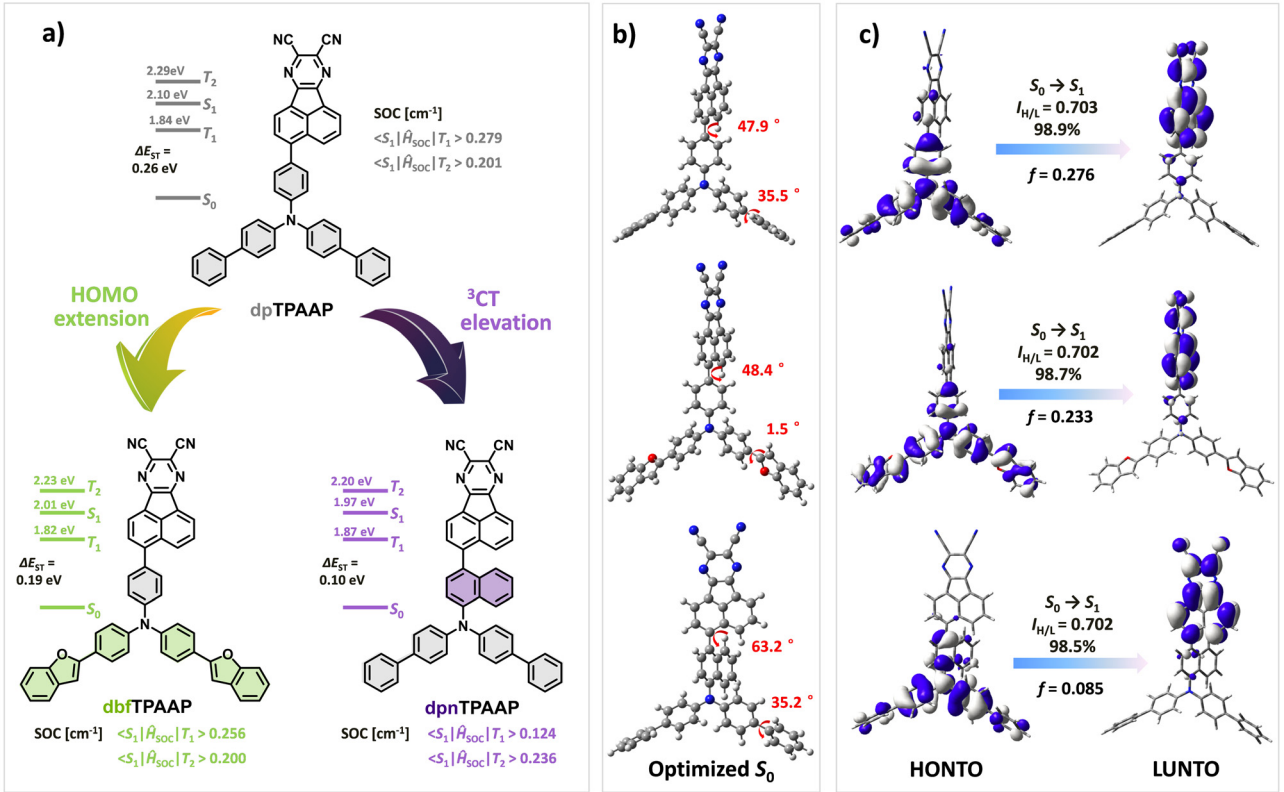

Fig. 1 (a) Schematic diagram of the fine-tuning strategy and the calculated TADF parameters of dbfTPAAP, dpnTPAAP and dpTPAAP. (b) Optimized geometrical structures of the investigated molecules at ground states, and (c) natural transition orbital analysis for $S_0 \rightarrow S_1$ excitations.

$S_0 \rightarrow S_1$ excitations,[45] while the drawbacks are a relatively large ΔE_{ST} and low k_{RISC} resulting in an inferior device efficiency.[46–48] With this in mind, precisely regulating the TADF parameters of triarylamine derivative based D–A type red/NIR emitters may offer a reliable means to further improve their electroluminescence (EL) performances.

To highlight the fine-tuning strategy, two new triarylamine based D adopted with acenaphtho[1,2-*b*]pyrazine-8,9-dicarbonitrile A, namely, dbfTPAAP and dpnTPAAP were elaborately designed and synthesized (Fig. 1a). In comparison with the previously reported dpTPAAP,[33] the altering of peripheral phenyl to benzofuryl on dbfTPAAP will be expected to extend their HOMO extension and afford enhanced intermolecular CT features, while the introduced naphthyl on dpnTPAAP will appropriately restrict the rotatable of π-bridge and output a smaller ΔE_{ST} and a higher k_{RISC}. Theoretical calculations fully confirm that both dbfTPAAP and dpnTPAAP demonstrate more balanced parameters than the reference dpTPAAP, *i.e.*, a small ΔE_{ST}, a high f and SOC value, which will facilitate a higher Φ_{PL} and exciton utilization. As expected, both dbfTPAAP and dpnTPAAP show bright pure red emission (~620 nm) in dilute toluene, along with an improved Φ_{PL} of 81% and 86% for dbfTPAAP and dpnTPAAP (3 wt% in 5-(3-(4,6-diphenyl-1,3,5-triazin-2-yl)phenyl)-7,7-dimethyl-5,7-dihydroindeno[2,1-*b*]-carbazole, DMIC-TRz matrix),[49] respectively. According to the transient photoluminescence (PL) decay curves, compared to the primary dpTPAAP, the k_{RISC}/k_{ISC}, and $k_{r,s}$/nonradiative decay rate ($k_{nr,s}$) values are enhanced 22% and 45% for dbfTPAAP and 78% and 163% for dpnTPAAP, respectively, which implies a reinforced ability to harvest triplet excitons. EL devices employing them as red/NIR emitters were fabricated; compared to the 15.1% (@630 nm) maximum external quantum efficiency (EQE_{max}) and turn-on voltage (V_{on}) of 2.4 V for the reference dpTPAAP, the EQE_{max} and V_{on} were remarkably improved to 18.1% (@632 nm)/2.3 V, and 18.9% (@630 nm)/2.3 V for dbfTPAAP and dpnTPAAP, respectively. In addition, even at a high doping concentration of 20 wt%, a high EQE_{max} of 12.6% (@680 nm) can be achieved by dpnTPAAP due to the balanced TADF parameters.

Initially, density functional theory (DFT) calculations using the Gaussian 16 program package at the B3LYP(D3BJ)/Def2-SVP level were performed.[50] As expected, all these three investigated TADF molecules show spatially separated HOMO and LUMO and resulting typical CT attribute of the S_1 (Fig. 1c). With the introduction of benzofuryl, the HOMO distribution of dbfTPAAP was obviously extended to the periphery of the D moiety, affording a 0.07 eV rise of the HOMO level and equally narrowing of ΔE_{ST} (Fig. 1a and Fig. S26, ESI†), which were beneficial for the RISC process and broadened intermolecular CT interactions. Meanwhile, the calculated SOC values of dbfTPAAP between the excited S_1 and T_1 $\langle S_1|\hat{H}_{SOC}|T_1\rangle$ (0.256 cm^{-1}) or S_1 and T_2 $\langle S_1|\hat{H}_{SOC}|T_2\rangle$ (0.200 cm^{-1}) as well as the dihedral angle (48.4°) between the D and A segments (Fig. 1b), and f values (0.233) for $S_0 \rightarrow S_1$ excitations (Fig. 1c) were comparable to those of the reference dpTPAAP. In stark contrast, the parameters relevant to the TADF path were

remarkably changed with the altering of the π-bridge to naphthyl, *i.e.*, a smaller ΔE_{ST} (0.10 eV), a higher T_1 level (^{3}CT, 1.87 eV), a larger dihedral angle (63.2°) but depressed SOC and *f* values (Fig. 1). To further investigate the impact on fluorescence efficiency along with the fine-tuning of TADF parameters, the Huang–Rhys factors (HRFs) at different vibration modes (ν) were calculated using MOMAP in the DUSHIN module.[51–53] As revealed in Fig. 2a, the dominated HRFs of $S_1 \rightarrow S_0$ on dpTPAAP involve both low-frequency twisting vibration modes (ν = 11.5 cm^{-1}) and high-frequency stretching vibrations that are associated with the fluctuations of bond length within different segments (*e.g.*, ν = 581.4, 687.3 and 789.5 cm^{-1}). Obviously, the introduction of the large steric hindrance naphthyl π-bridge can significantly restrain both the high- and low-frequency vibrations (Fig. 2b), and therefore the non-radiative energy consumptions of S_1 can be substantially suppressed,[54] while for dbfTPAAP, an additional swing vibration model (ν = 51.4 cm^{-1}) on the peripheral benzofuryl can be observed instead (Fig. 2c), indicating a negative effect to restrain the $k_{nr,s}$ from this point of view.

The synthetic routes to dbfTPAAP and dpnTPAAP are described in Scheme S1 (ESI†), and dpTPAAP was prepared according to a previous document.[33] The key intermediates of 5-(4-(bis(4-(benzofuran-2-yl)phenyl)amino)phenyl)acenaphthylene-1,2-dione (A3) and 5-(5-(di([1,1′-biphenyl]-4-yl)amino)naphthalen-1-yl)acenaphthylene-1,2-dione (B3) were synthesized by using a modified Suzuki–Miyaura cross-coupling reaction with a considerable yield of 76% and 56%, respectively. Thereafter, the acid catalyzed cyclization between the A3/B3 and 2,3-diaminomaleonitrile yielded the target compounds of dbfTPAAP and dpnTPAAP with good yields of 67% and 58%, respectively. The chemical structures of dbfTPAAP and dpnTPAAP were thoroughly characterized with ^{1}H NMR, ^{13}C NMR, and high resolution mass spectrometry (HRMS, APCI) (Fig. S1–S25, ESI†). All these compounds display favorable thermal stability with high decomposition temperatures (T_d, identified with 5% weight loss) of 489 °C (dbfTPAAP), 425 °C (dpnTPAAP) and 440 °C (dpTPAAP) according to the thermogravimetric analysis (Fig. S27, ESI†). Compared to the dpTPAAP (128 °C), the glass transition temperature (T_g) of dpnTPAAP was elevated to 184 °C, implying a more rigid structure conformation of the latter than the former (Fig. S28, ESI†). The experimental value of HOMO/LUMO levels was estimated from their onset potential of cyclic voltammetry curves (Fig. S29, ESI† and Table 1), *i.e.*, −5.15 eV/−3.47 eV for dbfTPAAP, −5.21 eV/−3.47 eV for dpnTPAAP and −5.19 eV/−3.46 eV for dpTPAAP, which were in line with the general trend of DFT results.

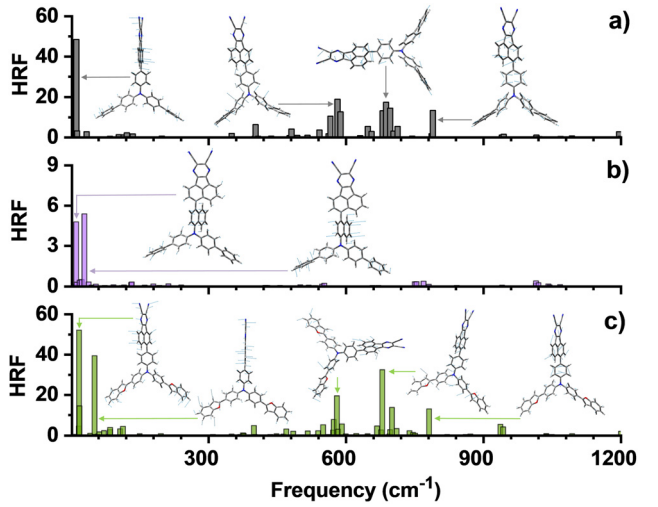

Fig. 2 The HRFs *versus* frequencies, and the relatively characteristic vibration modes for $S_1 \rightarrow S_0$ transition of (a) dpTPAAP, (b) dpnTPAAP and (c) dbfTPAAP.

Fig. 3 demonstrates the single-crystal structure of the dbfTPAAP and corresponding packing patterns. The dihedral angle between the D and A moieties is 41.15°, in accord with the DFT results (Fig. 3a), but distinct results can be observed between the triphenylamine fragment and the peripheral benzofuryls, which can be understood in terms of the differentiated intermolecular interactions. As displayed in Fig. 3b, the measured π–π distance between the A plane and one of the benzofuryl substituted triphenylamine legs is as small as 3.30 Å, implying strong intermolecular CT interactions between the aforementioned two planes. In addition, the measured C–H···N distance between the cyano group of A and the benzofuryl of the other triphenylamine legs is as short as 2.64 Å, which is within the coverage of the hydrogen bond. Therefore, such staggered intermolecular interactions among different monomers offer an enhanced CT feature within the *P*21/*n* space groups (Fig. 3c).

The photophysical properties of these emitters both in dilute toluene and film states were investigated and the results are shown in Fig. 4 and Table 1. As revealed in Fig. 4a, all the three emitters demonstrate two distinct absorption bands, *i.e.*, an intense high energy absorption band ranging from 300 to 400 nm assigned to the composition of π–π* and n–π* transitions of the D and A moieties, while the low energy absorption band at around 500 nm belongs to the typical intramolecular CT transitions from the D to the A segments Accordingly, an obvious redshift can be observed on these fluorescence emission spectra with the increase of solvent polarity (Fig. S30, ESI†), agreeing with the typical intermolecular CT transition feature. Compared to the dpTPAAP, the emission peaks of dbfTPAAP and dpnTPAAP in toluene were slightly red-shifted to 616 and 625 nm, respectively. All the three emitters demonstrate remarkably shifted emission peaks in neat films extending to the NIR region, but the peaks of both dbfTPAAP and dpTPAAP were larger than that of the dpnTPAAP due to the contribution of intermolecular CT transitions (inset of Fig. 4c). Steady state PL spectra of the doped films were collected in the DMIC-TRz matrix, and feedback deep-red emission of ~650 nm at 3 wt%, NIR emission of ~671 nm at 20 wt% (Fig. 4b).

To further investigate their TADF behaviors along with the fine-tuning of molecular parameters, transient PL decay curves of these emitters both in neat and doped films were measured. In comparison with the neat samples (Fig. 4c), all the three red/NIR TADF emitters distinctly exhibited a second-order exponential PL decay, consisting of a prompt component and a

Table 1 Photophysical and electrochemical properties of the three emitters

Emitter	λ_{abs}[a] [nm]	λ_{PL}[a] [nm]	E_{HOMO}/E_{LUMO}[b] [eV]	S_1/T_1[c] [eV]	ΔE_{ST}[d] [eV]	Φ_{PL}[e] [%]	Φ_p[f] [%]	Φ_d[f] [%]	τ_p[g] [ns]	τ_d[g] [μs]	$k_{r,s}$[h] [10^7 s^{-1}]	$k_{nr,s}$[h] [10^6 s^{-1}]	k_{ISC}[i] [10^7 s^{-1}]	k_{RISC}[i] [10^4 s^{-1}]
dbfTPAAP	500	616	−5.19/−3.46	2.26/2.16	0.10	81	49	32	20.6	48.7	1.9	4.5	2.5	2.6
dpnTPAAP	486	625	−5.21/−3.47	2.27/2.23	0.04	86	64	22	34.3	51.1	1.6	2.6	1.0	1.9
dpTPAAP	501	611	−5.15/−3.47	2.26/2.12	0.14	78	47	31	21.2	67.5	1.7	4.9	2.5	1.8

[a] Measured in 1×10^{-4} mol L^{-1} toluene solutions. [b] Calculated from the onset potential of cyclic voltammetry curves in the oxidation or reduction process. [c] Estimated from the onset of the fluorescence and phosphorescence spectra at 77 K, respectively. [d] $\Delta E_{ST} = S_1 - T_1$. [e] Total Φ_{PL} (3 wt% doped in DMIC-TRz). [f] Φ_{PL} contributions of the prompt component (p) and delayed (d) component, respectively. [g] The PL lifetimes of prompt (τ_p) and delayed (τ_d) decay components measured in 3 wt% doped DMIC-TRz film under an argon atmosphere. [h] Calculated $k_{r,s}$ and $k_{nr,s}$ values from S_1 to S_0. [i] Calculated ISC (k_{ISC}) and RISC (k_{RISC}) rate constants.

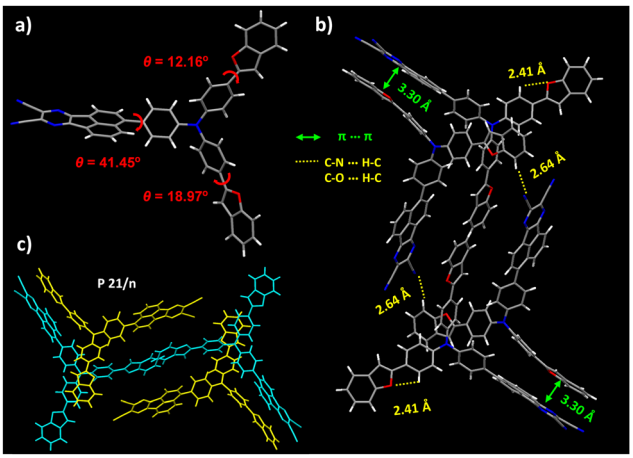

Fig. 3 (a) Single-crystal structure of the dbfTPAAP with solvent molecules omitted, (b) packing patterns in one space unit and (c) highlighted with two different colors.

delayed component (Fig. 4d). The fitted lifetimes (at 298 K) of the prompt (τ_p) and delayed (τ_d) components are 20.6 ns and 48.7 μs for dbfTPAAP, 34.3 ns and 51.1 μs for dpnTPAAP, and 21.2 ns and 67.5 μs for dpTPAAP, respectively (Fig. 3d and Fig. S32, ESI†). As expected, the delayed fluorescence components of all the three samples were enhanced distinctly with the temperature increase from 77 K to 298 K (Fig. 4d), conforming to the typical TADF behaviors.[40] Obviously, both the extension of HOMO delocalization and narrowing of the ΔE_{ST} value of the triphenylamine-based TADF molecules are beneficial for decreasing their τ_d values and therefore avoiding undesired quenching of triplet excitons in OLEDs. The Φ_{PL} of 3 wt% doped DMIC-TRz was collected as well, and slightly enhanced Φ_{PL} of 81% (dbfTPAAP) and 86% (dpnTPAAP) in contrast to the 78% (dpTPAAP) were obtained. According to the proportion of Φ_{PL} in prompt (Φ_p) or delayed fluorescence (Φ_d), the k_{ISC} and k_{RISC} of the three samples were estimated. Compared to the dpTPAAP, the k_{RISC} and k_{RISC}/k_{ISC} values of both dbfTPAAP and dpnTPAAP were remarkably optimized. In addition, the $k_{r,s}$ and $k_{r,s}/k_{nr,s}$ values are improved synchronously (Table 1), indicating a successful strategy *via* parameter optimization as well as preferable potential to adapt to the application in OLEDs.

To evaluate the EL properties of these red/NIR TADF emitters, vacuum evaporated multilayer OLEDs with the configuration of "ITO/HATCN (5 nm)/TAPC (30 nm)/TCTA (15 nm)/mCBP (10 nm)/EMLs (30 nm)/POT2T (20 nm)/ANT-BIZ (30 nm)/Liq (2 nm)/Al (100 nm)" were fabricated (Fig. 5a). Herein, the dipyrazino[2,3-*f*:2′,3′-*h*]quinoxaline-2,3,6,7,10,11-hexacarbonitrile (HATCN) with a deep LUMO level was incorporated as the hole injection layer, the 4,4′,4″-tris(carbazol-9-yl)triphenyl-amine (TCTA) and 1,1-bis((di-4-tolylamino)phenyl)-cyclohexane (TAPC) were employed as hole-transporting layers, and 1-(4-(10-([1,1′-biphenyl]-4-yl)anthracen-9-yl)phenyl)-2-ethyl-1*H*-benzo[*d*]imidazole (ANT-BIZ) was used as the electron-transporting layer. The 3,3-di(9*H*-carbazol-9-yl)biphenyl (mCBP) and (1,3,5-triazine-2,4,6-triyl)tris-(benzene-3,1-diyl)tris(diphenylphosphineoxide) (POT2T) were introduced as electron/hole blocking layers, respectively (Fig. 5b). The EMLs were composed of 3 wt% dbfTPAAP, 3 wt% dpnTPAAP, 3 wt% dpTPAAP or 20 wt% dpnTPAAP in the DMIC-TRz matrix, denoted as devices A, B, C and D respectively.

As revealed in Table 2, devices A–C with the same low dopant concentrations (3 wt% in DMIC-TRz) all display pure red-emission (EL peaks ~630 nm). Among the three devices, owing to the more balanced TADF parameters of the dbfTPAAP and dpnTPAAP than the dpTPAAP, the CE_{max}, PE_{max}, and EQE_{max} of devices A and B are obviously improved in contrat to the device C, which comforms to the higher key TADF parameters (k_{RISC}, k_{RISC}/k_{ISC}, $k_{r,s}$, $k_{r,s}/k_{nr,s}$ and Φ_{PL}) of the former two than the latter one. The optimal device performance was obtained by device B (dpnTPAAP) with an EQE_{max} of 18.9%, a CE_{max} of 21.6 cd A^{-1} and a PE_{max} of 28.2 lm W^{-1}, which represented a 25%, 37% and 36% improvement accordingly with reference to the device C (dpTPAAP). Moreover, slightly decreased V_{on} (0.1 V) of the devices A and B compared to the C can be observed as well (Fig. 5c), which may originate from the better matched energy levels or more balanced hole/electron transport of the dbfTPAAP and dpnTPAAP than the primary dpTPAAP. With the increase of loading of dpnTPAAP (20 wt% in DMIC-TRz, device D), the EL_{peak} significantly shifted to the deep-red region (680 nm), and a considerably high EQE_{max} of 12.6% can be maintained as well (Fig. 5d). Notably, all these devices demonstrate obvious efficiency roll-off at high brightness (Table 2), which can be ascribed to the typical triplet–triplet annihilation mechanism.[46] In addition, non-doped devices by employing the two new emitters were fabricated as well, and the emission peaks were successfully extended to the NIR region (~780 nm) together with a considerable EQE_{max} of around 1% (Fig. S33, ESI†).

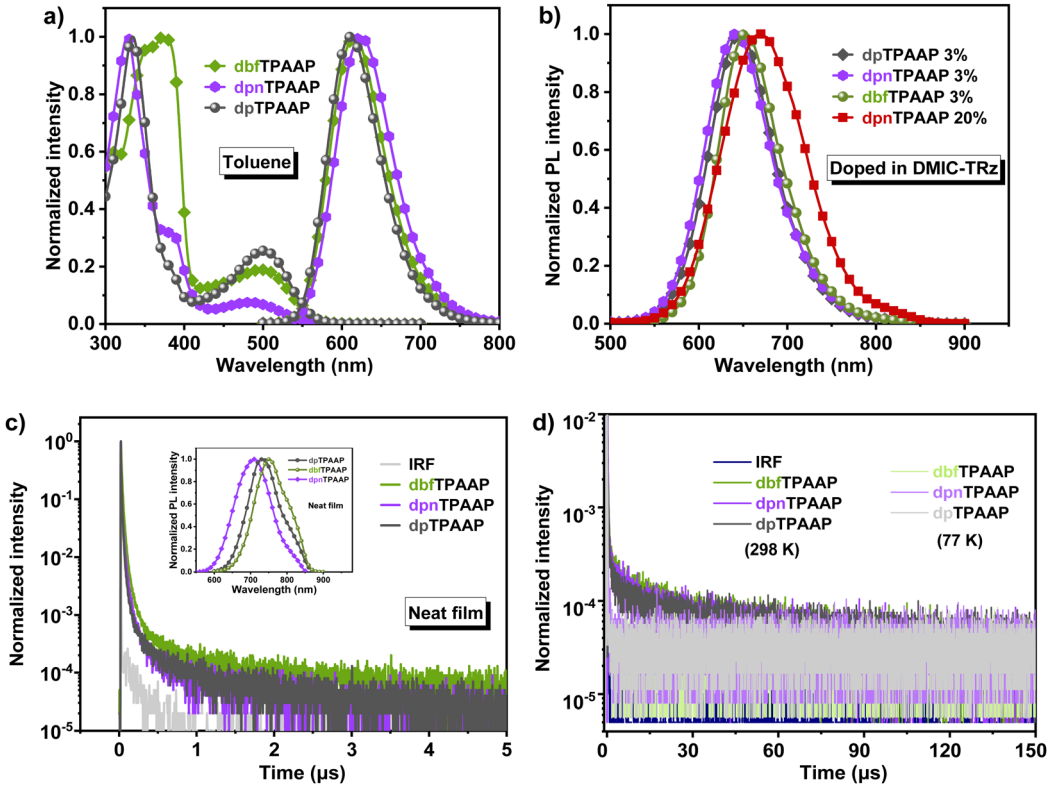

Fig. 4 (a) UV-Vis absorption and photoluminescence (PL) spectra of the dbfTPAAP, dpnTPAAP and dpTPAAP in dilute toluene (1×10^{-4} mol L^{-1}). (b) Steady state PL spectra of the doped films with 3 wt% or 20 wt% in the DMIC-TRz matrix. Transient PL decay curves of these emitters (c) in neat films, inset: PL spectra in neat films, and (d) in the DMIC-TRz (3 wt%) matrix at different temperatures (under an argon atmosphere).

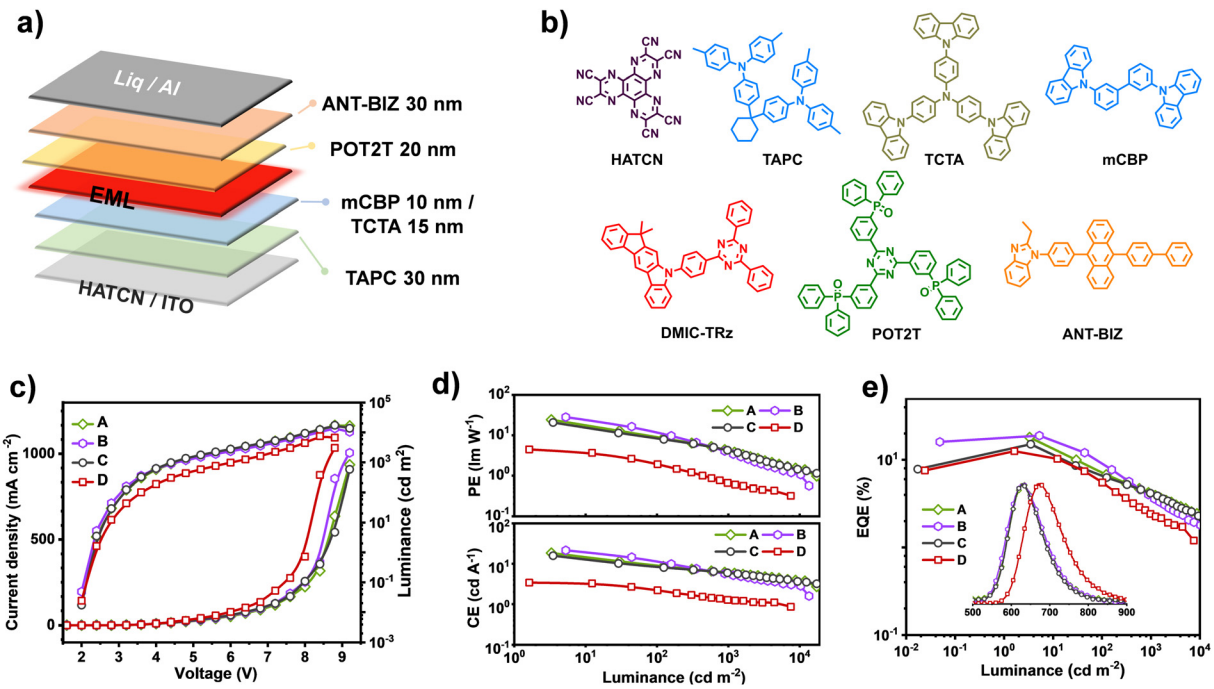

Fig. 5 (a) The diagram of OLED structures, and (b) chemical structures of the used materials. (c) The current density–voltage–luminance (*J*–*V*–*L*) curves of these devices. (d) Power efficiency and current efficiency as a function of luminance, and (e) EQE curves *versus* luminance, and EL spectra (inset, at the same driving voltage of 2.8 V) of these involved devices (A–D).

Table 2 EL performances of these involved devices

Devices	V_{on}[a] [V]	L_{max}[b] [cd m^{-2}]	CE_{max}[c] [cd A^{-1}]	PE_{max}[d] [Im W^{-1}]	EQE[e] [%]	EL_{peak}[f] [nm]
A	2.3	17 355	18.5	24.3	18.1/9.1/4.2	632
B	2.3	13 557	21.6	28.2	18.9/7.2/3.9	630
C	2.4	17 355	15.8	20.7	15.1/6.6/4.1	630
D	2.4	7523	3.4	4.5	12.6/5.6/2.4	680

[a] V_{on}, turn-on voltage at 1 cd m^{-2}. [b] L_{max}, the maximum luminance of the devices. [c] CE_{max}, the maximum current efficiency. [d] PE_{max}, the maximum power efficiency. [e] EQE values, following the sequence of maximum, at 100 cd m^{-2}, and at 1000 cd m^{-2},respectively. [f] The EL emission peaks at the same driving voltage of 2.8 V.

Conclusions

In conclusion, two new triarylamine based D–A type red/NIR TADF emitters with fine-tuning molecular parameters were elaborately designed and synthesized. In comparison with the model molecule of dpTPAAP, the incorporation of planar electron-rich end-capping groups (*i.e.*, benzofuryl) at the periphery of triarylamine legs can efficiently enlarge the HOMO distributions and subsequently strengthen their intermolecular CT interactions, while the suppression of nonradiative energy consumptions and synchronous increase of k_{RISC} can be realized by introducing a block π-bridge (*i.e.*, naphthyl). Notably, the fine-tuning strategy offers a directed way to predictably equilibrate the key TADF parameters and obtain desirable red/NIR TADF emitters with improved device performances. Consequently, EL devices employing these red/NIR emitters were fabricated, and an EQE_{max} approaching 20% (@ 630 nm, with 25% improvement in contrast to the reference one), or 12.6% (@680 nm) was achieved.

Conflicts of interest

There are no conflicts to declare.

Acknowledgements

This research was financially supported by the Natural Science Foundation of China (No. 51803124, 51903158 and 51903252), the Shenzhen Science and Technology Program (No. KQTD20170330110107046 and ZDSYS 20210623091813040), and Natural Science Foundation of Hubei Provincial (2021CFB398). The authors also thank the Instrumental Analysis Center of Shenzhen University for Analytical Support. They thank Kui Gong, Yibin Hu and Yin Wang (all from HZWTECH) for help and discussions regarding this study.

References

1 Y. Xu, P. Xu, D. Hu and Y. Ma, *Chem. Soc. Rev.*, 2021, **50**, 1030–1069.
2 J. Song, H. Lee, E. G. Jeong, K. C. Choi and S. Yoo, *Adv. Mater.*, 2020, **32**, 1907539.
3 G. Hong, X. Gan, C. Leonhardt, Z. Zhang, J. Seibert, J. M. Busch and S. Brase, *Adv. Mater.*, 2021, **33**, 2005630.
4 P. Jiang, J. Miao, X. Cao, H. Xia, K. Pan, T. Hua, X. Lv, Z. Huang, Y. Zou and C. Yang, *Adv. Mater.*, 2022, **34**, 2106954.
5 M. Yang, I. S. Park and T. Yasuda, *J. Am. Chem. Soc.*, 2020, **142**, 19468–19472.
6 X. Yin, G. Xie, Y. Peng, B. Wang, T. Chen, S. Li, W. Zhang, L. Wang and C. Yang, *Adv. Funct. Mater.*, 2017, **27**, 1700695.
7 X. Yin, T. Zhang, Q. Peng, T. Zhou, W. Zeng, Z. Zhu, G. Xie, F. Li, D. Ma and C. Yang, *J. Mater. Chem. C*, 2015, **3**, 7589–7596.
8 Y. J. Yu, X. Q. Wang, J. F. Liu, Z. Q. Jiang and L. S. Liao, *iScience*, 2021, **24**, 102123.
9 Y. Liu, C. Li, Z. Ren, S. Yan and M. R. Bryce, *Nat. Rev. Mater.*, 2018, **3**, 18020.
10 X. Cai, J. Xue, C. Li, B. Liang, A. Ying, Y. Tan, S. Gong and Y. Wang, *Angew. Chem., Int. Ed.*, 2022, **61**, 202200337.
11 X. K. Chen, D. Kim and J. L. Bredas, *Acc. Chem. Res.*, 2018, **51**, 2215–2224.
12 P. K. Samanta, D. Kim, V. Coropceanu and J. L. Bredas, *J. Am. Chem. Soc.*, 2017, **139**, 4042–4051.
13 X.-K. Chen, S.-F. Zhang, J.-X. Fan and A.-M. Ren, *J. Phys. Chem. C*, 2015, **119**, 9728–9733.
14 U. Balijapalli, Y. T. Lee, B. S. B. Karunathilaka, G. Tumen-Ulzii, M. Auffray, Y. Tsuchiya, H. Nakanotani and C. Adachi, *Angew. Chem., Int. Ed.*, 2021, **60**, 19364–19373.
15 S. Kothavale, W. J. Chung and J. Y. Lee, *J. Mater. Chem. C*, 2022, **10**, 6043–6049.
16 Y. Liu, J. Yang, Z. Mao, X. Chen, Z. Yang, X. Ge, X. Peng, J. Zhao, S. J. Su and Z. Chi, *ACS Appl. Mater. Interfaces*, 2022, **14**, 33606–33613.
17 Y.-C. Wei, S. F. Wang, Y. Hu, L.-S. Liao, D.-G. Chen, K.-H. Chang, C.-W. Wang, S.-H. Liu, W.-H. Chan, J.-L. Liao, W.-Y. Hung, T.-H. Wang, P.-T. Chen, H.-F. Hsu, Y. Chi and P.-T. Chou, *Nat. Photonics*, 2020, **14**, 570–577.
18 K. Zhang, X. Zhang, J. Fan, Y. Song, J. Fan, C. K. Wang and L. Lin, *J. Phys. Chem. Lett.*, 2022, **13**, 4711–4720.
19 R. Englman and J. Jortner, *Mol. Phys.*, 1970, **18**, 145–164.
20 Y. Zhang, D. Zhang, T. Huang, A. J. Gillett, Y. Liu, D. Hu, L. Cui, Z. Bin, G. Li, J. Wei and L. Duan, *Angew. Chem., Int. Ed.*, 2021, **60**, 20498–20503.
21 B. Zhao, H. Wang, C. Han, P. Ma, Z. Li, P. Chang and H. Xu, *Angew. Chem., Int. Ed.*, 2020, **59**, 19042–19047.
22 K. Tuong, Ly, R.-W. Chen-Cheng, H.-W. Lin, Y.-J. Shiau, S.-H. Liu, P.-T. Chou, C.-S. Tsao, Y.-C. Huang and Y. Chi, *Nat. Photonics*, 2016, **11**, 63–68.
23 A. Zampetti, A. Minotto and F. Cacialli, *Adv. Funct. Mater.*, 2019, **29**, 1807623.
24 J. H. Kim, J. H. Yun and J. Y. Lee, *Adv. Opt. Mater.*, 2018, **6**, 1800255.
25 Y. J. Yu, Y. Hu, S. Y. Yang, W. Luo, Y. Yuan, C. C. Peng, J. F. Liu, A. Khan, Z. Q. Jiang and L. S. Liao, *Angew. Chem., Int. Ed.*, 2020, **59**, 21578–21584.
26 H. Y. Zhang, H. Y. Yang, M. Zhang, H. Lin, S. L. Tao, C. J. Zheng and X. H. Zhang, *Mater. Horiz.*, 2022, **9**, 2425–2432.

27 U. Balijapalli, R. Nagata, N. Yamada, H. Nakanotani, M. Tanaka, A. D'Aléo, V. Placide, M. Mamada, Y. Tsuchiya and C. Adachi, *Angew. Chem., Int. Ed.*, 2021, **60**, 8477–8482.
28 J. X. Chen, W. W. Tao, W. C. Chen, Y. F. Xiao, K. Wang, C. Cao, J. Yu, S. Li, F. X. Geng, C. Adachi, C. S. Lee and X. H. Zhang, *Angew. Chem., Int. Ed.*, 2019, **58**, 14660–14665.
29 J. X. Chen, H. Wang, Y. F. Xiao, K. Wang, M. H. Zheng, W. C. Chen, L. Zhou, D. Hu, Y. Huo, C. S. Lee and X. H. Zhang, *Small*, 2022, **18**, 2201548.
30 P. Data, P. Pander, M. Okazaki, Y. Takeda, S. Minakata and A. P. Monkman, *Angew. Chem., Int. Ed.*, 2016, **55**, 5739–5744.
31 Y. Zhang, Y. Wang, J. Song, J. Qu, B. Li, W. Zhu and W.-Y. Wong, *Adv. Opt. Mater.*, 2018, **6**, 1800466.
32 J. Fan, J. Miao, N. Li, Y. Zeng, C. Ye, X. Yin and C. Yang, *J. Mater. Chem. C*, 2022, **10**, 10255–10261.
33 J. Xue, J. Xu, J. Ren, Q. Liang, Q. Ou, R. Wang, Z. Shuai and J. Qiao, *Sci. China: Chem.*, 2021, **64**, 1786–1795.
34 D.-H. Kim, A. D'Aléo, X.-K. Chen, A. D. S. Sandanayaka, D. Yao, L. Zhao, T. Komino, E. Zaborova, G. Canard, Y. Tsuchiya, E. Choi, J. W. Wu, F. Fages, J.-L. Brédas, J.-C. Ribierre and C. Adachi, *Nat. Photonics*, 2018, **12**, 98–104.
35 Z. Cai, X. Wu, H. Liu, J. Guo, D. Yang, D. Ma, Z. Zhao and B. Z. Tang, *Angew. Chem., Int. Ed.*, 2021, **60**, 23635–23640.
36 J. X. Chen, Y. F. Xiao, K. Wang, D. Sun, X. C. Fan, X. Zhang, M. Zhang, Y. Z. Shi, J. Yu, F. X. Geng, C. S. Lee and X. H. Zhang, *Angew. Chem., Int. Ed.*, 2021, **60**, 2478–2484.
37 U. Balijapalli, R. Nagata, N. Yamada, H. Nakanotani, M. Tanaka, A. D'Aleo, V. Placide, M. Mamada, Y. Tsuchiya and C. Adachi, *Angew. Chem., Int. Ed.*, 2021, **60**, 8477–8482.
38 Y. Xiao, H. Wang, Z. Xie, M. Shen, R. Huang, Y. Miao, G. Liu, T. Yu and W. Huang, *Chem. Sci.*, 2022, **13**, 8906–8923.
39 Y. Y. Wang, K. N. Tong, K. Zhang, C. H. Lu, X. Chen, J. X. Liang, C. K. Wang, C. C. Wu, M. K. Fung and J. Fan, *Mater. Horiz.*, 2021, **8**, 1297–1303.
40 Y. L. Zhang, Q. Ran, Q. Wang, Y. Liu, C. Hanisch, S. Reineke, J. Fan and L. S. Liao, *Adv. Mater.*, 2019, **31**, 1902368.
41 J. Liu, Z. Li, T. Hu, T. Gao, Y. Yi, P. Wang and Y. Wang, *Adv. Opt. Mater.*, 2022, **10**, 2102558.
42 M. Zhao, M. Li, W. Li, S. Du, Z. Chen, M. Luo, Y. Qiu, X. Lu, S. Yang, Z. Wang, J. Zhang, S. J. Su and Z. Ge, *Angew. Chem., Int. Ed.*, 2022, 202210687.
43 D. G. Congrave, B. H. Drummond, P. J. Conaghan, H. Francis, S. T. E. Jones, C. P. Grey, N. C. Greenham, D. Credgington and H. Bronstein, *J. Am. Chem. Soc.*, 2019, **141**, 18390–18394.
44 Z. Li, D. Yang, C. Han, B. Zhao, H. Wang, Y. Man, P. Ma, P. Chang, D. Ma and H. Xu, *Angew. Chem., Int. Ed.*, 2021, **60**, 14846–14851.
45 J. Jiang, Z. Xu, J. Zhou, M. Hanif, Q. Jiang, D. Hu, R. Zhao, C. Wang, L. Liu, D. Ma, Y. Ma and Y. Cao, *Chem. Mater.*, 2019, **31**, 6499–6505.
46 H.-Y. Yang, H.-y Zhang, M. Zhang, X.-c Fan, H. Lin, S.-L. Tao, C.-J. Zheng and X.-H. Zhang, *Chem. Eng. J.*, 2022, **448**, 137717.
47 J. Xue, Q. Liang, R. Wang, J. Hou, W. Li, Q. Peng, Z. Shuai and J. Qiao, *Adv. Mater.*, 2019, **31**, 1808242.
48 C. Li, R. Duan, B. Liang, G. Han, S. Wang, K. Ye, Y. Liu, Y. Yi and Y. Wang, *Angew. Chem., Int. Ed.*, 2017, **56**, 11525–11529.
49 X. Lv, R. Huang, S. Sun, Q. Zhang, S. Xiang, S. Ye, P. Leng, F. B. Dias and L. Wang, *ACS Appl. Mater. Interfaces*, 2019, **11**, 10758–10767.
50 G. W. T. M. J. Frisch, H. B. Schlegel, G. E. Scuseria, J. R. C. M. A. Robb, G. Scalmani, V. Barone, H. N. G. A. Petersson, X. Li, M. Caricato, A. V. Marenich, B. G. J. J. Bloino, R. Gomperts, B. Mennucci, H. P. Hratchian, A. F. I. J. V. Ortiz, J. L. Sonnenberg, D. Williams-Young, F. L. F. Ding, F. Egidi, J. Goings, B. Peng, A. Petrone, D. R. T. Henderson, V. G. Zakrzewski, J. Gao, N. Rega, W. L. G. Zheng, M. Hada, M. Ehara, K. Toyota, R. Fukuda, M. I. J. Hasegawa, T. Nakajima, Y. Honda, O. Kitao, H. Nakai, K. T. T. Vreven, J. A. Montgomery Jr., J. E. Peralta, M. J. B. F. Ogliaro, J. J. Heyd, E. N. Brothers, K. N. Kudin, T. A. K. V. N. Staroverov, R. Kobayashi, J. Normand, A. P. R. K. Raghavachari, J. C. Burant, S. S. Iyengar, M. C. J. Tomasi, J. M. Millam, M. Klene, C. Adamo, R. Cammi, R. L. M. J. W. Ochterski, K. Morokuma, O. Farkas and A. D. J. F. J. B. Foresman, *Gaussian 16, Revision A.03*, Gaussian, Inc.: Wallingford CT, 2016.
51 Z. Shuai, *Chin. J. Chem.*, 2020, **38**, 1223–1232.
52 Z. Shuai and Q. Peng, *Nat. Sci. Rev.*, 2017, **4**, 224–239.
53 Z. Shuai and Q. Peng, *Phys. Rep.*, 2014, **537**, 123–156.
54 J. Fan, Y. Zhang, Y. Zhou, L. Lin and C.-K. Wang, *J. Phys. Chem. C*, 2018, **122**, 2358–2366.